Catalysis Today xxx (xxxx) xxx–xxx

Contents lists available at ScienceDirect

Catalysis Today

journal homepage: www.elsevier.com/locate/cattod

Hydrogen-rich gas production by steam and oxidative steam reforming of crude glycerol over Ni-La-Me mixed oxide catalysts (Me = Ce and/or Zr)

Santiago Veiga[a,*], Mariano Romero[b], Ricardo Faccio[b], Darío Segobia[c], Hernán Duarte[c], Carlos Apesteguía[c], Juan Bussi[a]

[a] Laboratorio de Fisicoquímica de Superficies, DETEMA, Facultad de Química, Universidad de la República, General Flores 2124, Montevideo, 11800, Uruguay
[b] Centro NanoMat/CryssMat-Lab, DETEMA, Facultad de Química, Universidad de la República, General Flores 2124, Montevideo, 11800, Uruguay
[c] Catalysis Science and Engineering Research Group (GICIC), INCAPE, UNL-CONICET, Predio CCT Conicet, Paraje El Pozo, Santa Fe, 3000, Argentina

ARTICLE INFO

Keywords:
Crude glycerol
Hydrogen
Nickel catalysts
Steam reforming

ABSTRACT

The production of H_2-rich gaseous mixtures from steam and oxidative steam reforming of crude glycerol was investigated on catalysts with general formula Ni(12 wt.%)-$La_2(Ce_{1-x}Zr_x)_2O_7$ (x = 0, 0.5, 1). The catalysts were prepared by the polymerized complex method based on the Pechini-type reaction route and characterized by a variety of physical and spectroscopic techniques. Samples were calcined in air at 850 °C for 4 h. All catalysts showed a well-defined NiO phase and a mixed oxide with a general formula $A_2B_2O_7$ (A: La; B: Ce and/or Zr). NiO was completely reduced to metallic Ni on all catalysts under pure H_2 at 650 °C. Ni reducibility is favored by the presence of Ce. Redox properties of Ce can also explain a synergetic effect leading to the higher basicity of the catalyst containing Ce and Zr (x = 0.5). Catalytic tests were performed at 650 °C by feeding the fixed-bed tubular reactor with a crude glycerol:water solution containing 30 wt% glycerol. The best results were achieved on the catalyst displaying the highest basicity (Ni-$La_2(Ce_{0.5}Zr_{0.5})_2O_7$ both under steam and oxidative reforming conditions. Removal of carbon and alkali metals by simple procedures allows to a significant recovery of the initial catalytic activity without changes in their chemical and phase structure.

1. Introduction

Over the past century, human activities have released large amounts of carbon dioxide and other greenhouse gases to the atmosphere thus contributing to the increase of earth's surface temperature beyond its historical average values, with potentially harmful effects on ecosystems, biodiversity and the livelihoods of people worldwide.

Since most greenhouse gases come from burning fossil fuels to produce energy, a transition towards a renewable, efficient and sustainable energy model based in the use of renewable energy is being adopted as a suitable strategy to mitigate the global warming impacts. In this sense, biomass-derived fuels have emerged as a suitable step and many countries have introduced advanced policies to support their production [1].

Biodiesel is one of the most popular biofuels and it is forecasted that it could make up a large fraction of all transportation fuels in the near future [2,3]. This biofuel presents some advantages compared to fossil fuels, such as its biodegradability, less carbon monoxide, particulate matter and polycyclic aromatic hydrocarbons (PAHs) emissions. However, biodiesel is not competitive in terms of price yet [4]. At present, biodiesel is commonly produced by transesterification of vegetable oils (canola, sunflower, palm, etc) or animal fat, with alcohol, usually methanol, in the presence of an alkali or acid homogeneous catalyst [5]. The products, fatty acid methylesters (FAMEs), are called biodiesel and include glycerol as a by-product. The transesterification reaction produces biodiesel and glycerol at a volumetric ratio of 10:1. This glycerol known as crude glycerol (CG) contains impurities such as methanol, water, inorganic salts, free fatty acids, mono-, di- and triacylglycerols and biodiesel making it a low value product. Because of that and also of the increasing worldwide biodiesel production this low-grade CG has become a significant problem concerning its final disposal. At present, CG is mainly incinerated to generate heat and electricity. This practice leads to the generation of greenhouse gases and an underutilization of the resource [6]. One way of lowering the production cost of biodiesel would be to use CG to produce a hydrogen-rich gas mixture via steam reforming, partial oxidation, autothermal or aqueous reforming techniques [7]. Steam reforming is the most widely used process to obtain hydrogen-rich mixtures from natural gas. This alternative is promising for the use of glycerol, since the processing of glycerol by catalytic reforming requires few changes in the industrial processes [7]. The

* Corresponding author.
E-mail address: sveiga@fq.edu.uy (S. Veiga).

https://doi.org/10.1016/j.cattod.2019.02.008
Received 8 May 2018; Received in revised form 14 December 2018; Accepted 10 February 2019
0920-5861/

addition of oxygen to steam reforming reaction converts the process into oxidative steam reforming of glycerol that could be an autothermic reaction. This oxygen decreases the risk of carbon deposition on the surface of the catalyst or acts to oxidize the already deposited carbon, regenerating the catalyst, thus maintaining the activity of the catalyst for a longer time [8]. Thermodynamic studies performed with pure glycerol showed that the most suitable conditions for H_2 production are attained at temperatures between 627–727 °C, water to glycerol ratios of 9 to 12 and oxygen to glycerol ratios of 0–0.4 [9]. However, very few studies have been conducted using CG in the feed probably because the catalyst is rapidly deactivated by the impurities contained in the CG. Slinn et al. [10] studied steam reforming of CG using Pt/Al_2O_3 over a range of conditions. A comparison between crude and pure glycerol was established. It was found that CG conversions were lower than those obtained with pure glycerol. They reported that long chain fatty acid impurities were harder to reform and more amount of carbon is deposited onto the catalyst surface. Dou et al. [11] investigated pure and CG steam reforming over a commercial Ni-based catalyst with and without in situ CO_2 removal by carbonation of calcined dolomite. The results indicated that steam reforming of CG with in situ CO_2 removal is shown to be an effective means of achieving hydrogen purity close to 90% in pre-CO_2 breakthrough conditions. Fermoso et al. [12] also studied CG steam reforming with in situ CO_2 removal (sorption enhanced steam reforming) but over Ni-Co catalyst derived from hydrotalcite-like material and calcined dolomite as CO_2 sorbent. This process occurred until the calcined dolomite was saturated (140 min). They concluded that the main challenges in CG steam reforming were carbon formation due to the presence of non-volatile heavy compounds and accumulation of alkaline salts due to the presence of transesterification catalysts in the CG. However, the effects of inorganic salts on long-term experiments was not investigated. Remón et al. [13] investigated the effect of acetic acid, methanol and potassium hydroxide on the catalytic steam reforming of glycerol. The results indicated that the impurities mentioned above strongly affect carbon conversion to gas and solid but the composition of the gas was barely affected by the presence of its. Remón et al. [14] also presented a two-step process for CG valorisation for hydrogen production using Ni-based catalysts in a fluidised bed reactor. The CG was first neutralised with acetic acid followed by a vacuum distillation to produce the refined glycerol, and then went through a catalytic steam reforming process. They found optimum conditions using a final pH of 6 in the neutralisation step, a temperature of 680 °C and a glycerol concentration of 37 wt.% in the refined glycerol solution. In a previous work we reported that activated carbon supported nickel catalysts were active in CG steam reforming at 650 °C. Promotion with different metal oxides (MgO, La_2O_3, Y_2O_3) was effective to increase H_2 yield which attains more than 80% of the maximum theoretical amount with MgO [15].

In another work of our group [16], Ni-La-Ti coprecipitated catalysts were evaluated in GC steam reforming at 500 °C and 650 °C. Carbon conversion to gas at 500 °C were ˜35% revealing a low decomposition of the different reaction intermediates through reactions with rupture of C—C bonds. At 650 °C conversion increased significantly (˜92.0%), which suggests that, in addition to the most reactive components (methanol and glycerol), fatty acids could also react under these reaction conditions leading to typical gaseous products.

The above results show that there is a still great challenge to produce almost pure hydrogen directly from CG due to the complexity of its composition.

Nickel is the most investigated metal in glycerol steam reforming because of its capacity to facilitate C-C rupture and its low cost compared to other metals also used for these purposes (Pt, Ru, Rh) [17–19].

The nature of the support plays an important role towards catalyst properties including its deactivation behavior. α-Al_2O_3 is the most commonly used due to its high specific surface area and its mechanical and chemical resistance under reaction conditions. However, it is also known that carbon deposition and catalyst sintering, both factor leading to catalyst deactivation are also promoted when alumina is used as support [19,20]. Other metal oxides are also used either as supports or promoters in order to improve the catalytic performance. ZrO_2 and CeO_2 are among the most investigated because of their capacity to increase resistance to carbon deposition and structural stability [21–29]. Favorable redox properties and oxygen mobility characteristics of these oxides allows them to supply oxygen to the active site and minimize carbon deposition and metal sintering.

Addition of several lanthanide and alkaline-earth metal cations such as Y^{3+}, La^{3+}, Ca^{2+}, and Mg^{2+} into these oxides also enhance the catalytic activity and resistance towards carbon deposition, which is ascribed to the improvement of structural stability and strong interactions with Ni [22,30,31]. In the case of La, MeO_2–La_2O_3 solid solutions (Me: Zr or Ce) with a crystalline structure typical of pyrochlore compounds are formed [32–34], while Ni is found as a NiO separate phase. Reduction of NiO to Ni is almost complete under operation conditions and strong interactions between both phases help to keep low Ni crystallite size and to avoid carbon accumulation.

In this work, mixed oxides of general formula Ni (wt. 12%)-$La_2(Zr_{1-x}Ce_x)_2$ were taken as precursors of Ni catalysts for an experimental investigation of steam and oxidative steam reforming of CG without any purification pretreatment. Zirconium substitution by cerium cations (x = 0.5) was evaluated in order to observe changes in catalytic activity and resistance to deactivation aiming at contributing to the scarce discussion of carbon formation when processing CG to generate green hydrogen.

2. Experimental

2.1. Materials

The materials used in this work were: zirconium n-propoxide [$Zr(OCH_2CH_2CH_3)_4$], 70% in 1-propanol (Aldrich, 97% purity), nickel, lanthanum and cerium nitrates [$Ni(NO_3)_2.6H_2O$, $La(NO_3)_3.6H_2O$, $Ce(NO_3)_3.6H_2O$] (Aldrich, 99% purity), citric acid monohydrate (Merck, 99.5 purity) and ethylene glycol (Carlo Erba, 99.5% purity).

2.2. Catalysts preparation

The synthesis was carried out by the Pechini-type polymerized complex route [35]. This technique allows preparing homogeneous complex oxides with perovskite, pyrochlore and fluorite structure having well controlled properties and it was used for several authors to synthesize steam reforming catalysts [36].

Three catalysts were prepared with the following metals atomic ratio: La:Ce = 1:1, La:Zr = 1:1 and La:Ce:Zr = 1:0.5:0.5. Ni content was 12 wt. % in all cases. The amount of nickel was selected according to other works that use Ni-based catalysts for glycerol steam reforming [4].

First, stoichiometric amounts of metal precursors were dissolved in ethylene glycol and then anhydrous citric acid (CA) was added to this solution. It was used a molar ratio of metal:CA of 1:3 and EG:CA of 4:1. The solution was stirred and heated to 70 °C for 1 h until it became translucent. After that, the temperature was increased to 130 °C to promote the polyesterification reaction between the citric acid and ethylene glycol. After several hours a transparent brown glassy resin was obtained which was then transferred to a muffle furnace at 350 °C for 2 h. The resulting black solid mass was carefully ground into a powder and subsequently calcined at 850 °C for 4 h. This calcination temperature was chosen to guarantee the formation of the biphasic system NiO/mixed oxide [37]. The three prepared catalysts will be denoted as NiLaCe, NiLaCeZr and NiLaZr for its identification in the rest of this work.

2.3. Catalyst characterization

Nitrogen physisorption measurements were conducted on a Beckman Coulter surface area analyzer (Coulter SA model 3100). The catalyst was degassed at 100 °C for 10 h prior to N_2 adsorption–desorption measurements. The specific surface area was calculated from the BET model and the total pore volume was estimated at a relative pressure of 0.98.

The crystalline phases of fresh and reduced catalysts were characterized with X-ray diffraction (XRD) using a Rigaku Ultima IV diffractometer with CuK_α radiation in the 2θ = 10–80° range using 2θ steps of 0.02° with a 5 s integration time per step. Ni and NiO crystallite size were estimated by the Scherrer equation [29].

The reducibility of the catalyst was studied by temperature programmed reduction (TPR) using 5% H_2/Ar at a flow rate of 60 $cm^3\,min^{-1}$. Standard reduction was conducted at a heating rate of 10 °C min^{-1} from 25 to 850 °C A mass spectrometer in a Baltzers Omnistar unit monitored the hydrogen consumption. Ni content in the catalysts were obtained by atomic emission spectroscopy coupled to an Inductively Coupled Plasma (ICP-OES) equipment Perkin-Elmer Optima 2100. Ni dispersion was determined by H_2 chemisorption in a volumetric equipment at 25 °C, using the double isotherm method assuming an adsorption stoichiometry of 1:1 as described in [30]. The catalyst sample was previously reduced in a pure H_2 flow at 650 °C and subsequently evacuated at the same temperature.

Basicity measurements were performed by temperature programmed desorption of CO_2 (TPD-CO_2) preadsorbed at room temperature. Reduced catalysts were exposed to a flowing mixture of 3% of CO_2 in N_2 (60 mL min^{-1}) until surface saturation. Then, weakly adsorbed CO_2 was removed by flushing with N_2. Finally, the temperature was increased to 800 °C at a ramp rate of 10 °C/min. The desorbed CO_2 was converted into CH_4 on a Ni/Kieselghur catalyst held at 400 °C and then analyzed in a flame ionization detector (FID).

Temperature-programmed oxidation (TPO) of the spent catalysts was carried out using a similar apparatus by introducing a gas flow (60 mL min^{-1}) containing a mixture of O_2:N_2 (2:98) and the temperature was increased up to 800 °C at a heating rate of 10 °C/min.

Carbon build-up on the spent catalysts was analysed for its C and H contents (Thermo Scientific Flash 2000).

EDS microanalysis of the tested catalysts were studied using scanning electron microscopy (Jeol JSM-5900 LV).

2.4. Crude glycerol

The CG used in the present work mainly consists of 64 wt% glycerol, inorganic salts 5.7 wt%, methanol and water lower than 5 wt% and fatty acids either free or as methyl esters up to 26 wt%, provided by ALUR (Alcoholes del Uruguay). Potassium methylate was used as transesterification catalyst. CG composition was determined by elemental analysis (Thermo Scientific Flash 2000) and it is recently reported elsewhere [15]. The calculated average elemental molar formula for CG determined from these results was $C_{3.5}H_{9.0}O_{3.1}$ and subsequently used to calculate conversion and yield parameters.

2.5. Catalytic tests

Crude glycerol steam reforming (CGSR) and oxidative steam reforming (CGOSR) tests were carried out in a 1.2 cm diameter and 30 cm length stainless steel tubular fixed bed reactor located inside a tubular electric furnace. The catalyst bed configuration consists in a 2 g SiC (30–40 mesh) bed placed above 0.2 g (120–170 mesh) of the catalyst. Before reaction, the catalyst was reduced under a 30 mL min^{-1} pure hydrogen flow by heating from room temperature to 650 °C, at a rate of 10 °C min^{-1} and keeping the final temperature for 1 h. The reduction temperature was chosen as the minimum in which the three catalysts are completely reduced. This was verified by performing a TPR of the reduced catalyst and verifying that the consumption of hydrogen corresponds only to the support. Following reduction, the H_2 flow was stopped and the reactor purged with argon. Then the reactor was brought to the reaction temperature under argon. After that, the water:CG solution (30 wt% of CG) was fed at 2.0 mL h^{-1} with a peristaltic pump (Cole Parmer 74900 Series) through a device consisting of two concentric tubes which are placed into the tubular reactor. Water:CG solution was injected into the internal tube (0.2 mm i.d.) and argon through the external one (2.1 mm i.d.). With this device, partial vaporization of glycerol and other compounds in the CG would occur in the sprayed liquid solution along with water. Proper adjustment of the distance of the device to the catalytic bed allowed to obtain a stable feed of the solution. Oxygen was fed through a separate gas line with an O_2 to CG molar ratio of 0.5. The experiments were performed at atmospheric pressure with time-on-stream (TOS) of 6 h and reaction temperature of 650 °C. Reaction temperature was chosen from a previous work in which pure glycerol was completely converted [34].

The steam-to-carbon (S/C) molar ratio was equal to 3.7. Under these conditions the gas hourly space velocity (GHSV) was 20 L $h^{-1}\,g^{-1}$ and $WHSV_{CG}$ defined as the ratio between the mass flow rate of crude glycerol fed and the mass of catalyst was 3 h^{-1}. Unreacted glycerol and some of the condensable reaction products were retained in a dry ice trap at the reactor exit. Three reaction cycles of 20 h making intermediates steps of regeneration were performed with the NiLaCeZr catalyst under GHSV = 35 L $h^{-1}\,g^{-1}$ and $WHSV_{CG}$ = 10 h^{-1} conditions. After the first cycle, regeneration was carried out at 650 °C for 1 h under 50% O_2/Ar atmosphere (20 mL min^{-1}). After the second cycle the catalyst was regenerated by treatment with oxygen and then washed with distilled water to remove the salts deposited on it.

Non-condensable products, H_2, CO, CO_2, CH_4, C_2 (ethane and ethylene) and C_3 (propane and propylene) hydrocarbons, were periodically analyzed with a gas-chromatograph (Shimadzu GC-14B) equipped with FID and TCD detectors in series and columns Supelco CarboxenTM-1000 and Porapak Q. At the end of reaction, glycerol and condensed liquid products were collected and analyzed by HPLC (Shimadzu Prominence) equipped with a Rezex RHM-Monosaccharide H+ (8%) column and a refractive index detector.

Catalytic performance was evaluated in terms of glycerol conversion, carbon conversion to non-condensable products ($X_{C,GAS}$), carbon conversion to liquid products ($X_{C,LIQ}$), hydrogen yield (H_2 yield) and product distribution (in dry basis) according to:

$$X_{Gly}(\%) = 100 * \frac{Gly_{in} - Gly_{out}}{Gly_{in}} \quad (1)$$

$$X_{C,GAS}(\%) = 100 * \frac{\sum F_{C,i} * n_i}{F_{C,IN}} \quad (2)$$

$$X_{C,LIQ}(\%) = 100 * \frac{C_{liq.\,products}\,(g)}{C_{FED}\,(g)} \quad (3)$$

$$H_2\ Yield\ (\%) = 100 * \left(\frac{F_{H_2}}{N_{TERMO} * F_{CG}}\right) \quad (4)$$

$$Y_i = 100 * \left(\frac{F_{C,i}\ or\ F_{H_2}}{\sum F_{C,i} + F_{H_2}}\right)(drybasis) \quad (5)$$

where $F_{C,i}$ is the molar flow of product i (i = CO, CO_2, CH_4, C_2H_4, C_2H_6, C_3H_6, C_3H_8); n_i the number of carbon atoms in product i; $F_{C,IN}$ is the molar flow of carbon atoms in the CG-water solution fed to the reactor and calculated over the 94.3% of the total weighted amount of CG used for its preparation (5.7% corresponds to the ash fraction determined by calcination); $C_{liq,\ products}$ is the total mass of carbon in products retained in the liquid aqueous solution in the dry ice trap (excluding glycerol); C_{FED} is the total mass of carbon in the CG-water solution fed during the test; F_{H2} is the molar flow rate of H_2 (mol min^{-1}); F_{CG} is the molar flow rate of CG (mol min^{-1}) and N_{TERMO} is the thermodynamic equilibrium

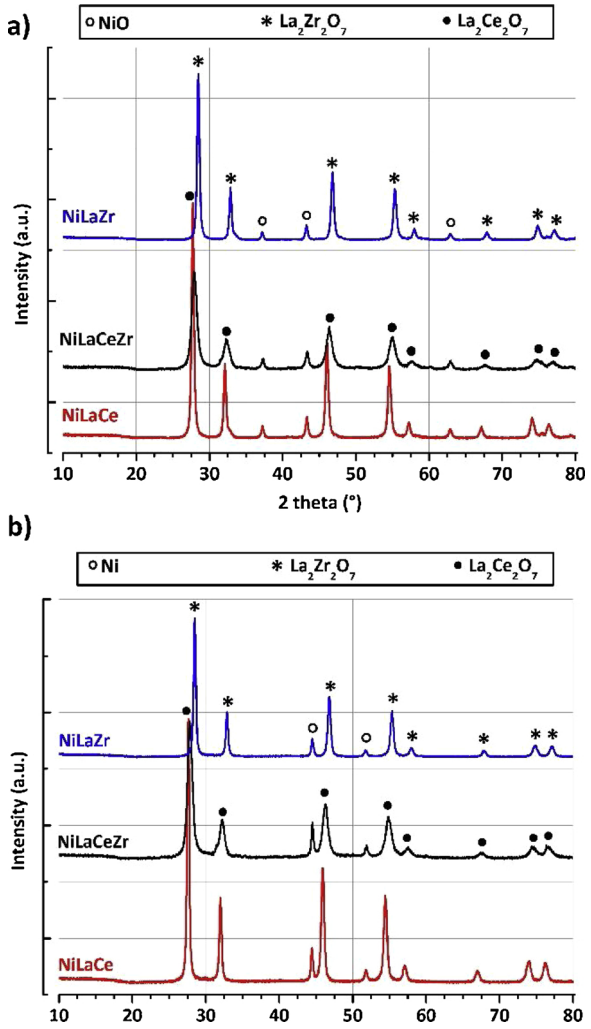

Fig. 1. XRD diffractograms of Ni-La-Me catalysts: (a) calcined; (b) reduced.

value of H_2 calculated by Fact-Web software [38] on the basis of Gibbs energy minimization, being 7.43 for CGSR and 6.55 for CGOSR.

Preliminary runs were carried out to determine the proper catalyst particle size and reactant flow to avoid internal and external diffusion limitations, respectively.

3. Results and discussion

The crystalline phases of fresh and reduced Ni-La-Me catalysts were identified determined by XRD. Diffractograms of the three calcined catalysts presented in Fig. 1a showed peaks at 2θ = 37.3°, 43.3° and 62.9° assigned to (111), (200), and (220) planes of cubic NiO phase. For NiLaCe catalyst peaks are corresponded to the pure $La_2Ce_2O_7$ phase in agreement with the literature [39]. NiLaZr catalyst peaks attributed to $La_2Zr_2O_7$ pyrochlore phase. The XRD pattern of the NiLaCeZr catalyst showed diffraction peaks shifted to higher and lower 2θ angles for $La_2Ce_2O_7$ and $La_2Zr_2O_7$ respectively in concordance with the lower ionic radii of Zr^{4+} (0.84 Å) with respect to the ionic radii of Ce^{4+} (0.97 Å) [34] indicating that Ce^{4+} and Zr^{4+} are replaced by each other [39]. Similar XRD patterns were observed over the reduced catalysts (Fig. 1b) in which the peaks corresponding to NiO disappears completely and peaks assigned to metallic nickel at 2θ = 44.5° and 51.8° corresponding to (111) and (200) planes appears, reflecting that nickel oxide was successfully reduced to metallic nickel. No diffraction peaks corresponding to La_2O_3, CeO_2 and ZrO_2 were detected in either the calcined or the reduced catalysts.

Table 1
Physicochemical properties of Ni-La-Me fresh calcined catalysts.

Catalyst	BET area ($m^2\,g^{-1}$)	Pore volume ($cm^3\,g^{-1}$)	Average pore diameter (nm)	Ni loading (wt. %)	NiO particle size[a] (nm)
NiLaCe	6.1	0.050	32.6	11.7	20
NiLaCeZr	12.7	0.075	23.7	11.7	19
NiLaZr	7.3	0.039	21.5	11.7	18

[a] Calculated by the Scherrer equation from the (200) diffraction peak of NiO XRD pattern.

The BET surface areas of the fresh catalysts were measured by N_2 physisorption, the results of which are presented in Table 1. Low BET areas were found for the 3 catalysts and are similar to those already reported in previous works for others trimetallic mixed oxide systems prepared by a coprecipitation technique [16,34]. Beyond the precedent comments, the BET area of NiLaCeZr practically doubles those of the two other catalysts. This catalyst also has the highest pore volume (0.075 $cm^3\,g^{-1}$) while NiLaZr has the smallest one. Differences between average pore diameters can also be observed with the highest value corresponding to NiLaCe (32.6 nm) and the smallest one to NiLaZr (21.5 nm). High calcination temperature (850 °C) used in the final thermal treatment probably leads to sintering of this type of solids, resulting in a large grain size with lower surface area. Table 1 also shows that Ni content are close to the theoretical value (12%). NiO particle size calculated by Scherrer´s equation was almost the same for the three prepared catalysts

Ni particle size was calculated from the Scherrer equation and by H_2 chemisorption measurements and the results are summarized in Table 2. The Scherrer equation provides very similar values (18–20 nm) while H_2 chemisorption provides quite different values. This last technique is pointed as the most suitable one since results are based on surface averaged particle size, while Scherrer equation provides results based on a volumetric basis [40]. NiLaZr has the smallest value with both calculation methods (D_{Ni} = 18 nm and 41 nm respectively), while NiLaCe has the highest one (20 and 112 nm). Based in results obtained by H_2 chemisorption a marked decrease is observed for the two Zr-containing catalysts with regards to the Zr-free one and that can be related to some properties of ZrO_2 materials. Indeed, it is well-known that ZrO_2 prevents Ni particles from sintering during the SR reactions at high temperatures [28,41]. This property can be related to its low thermal conductivity which allows it to be commonly used in thermal barrier coating materials [42]. The presence of ZrO_2 could thus depress thermal diffusion of different metal atoms in the bulk material thus slowing down Ni sintering. On the other hand, zirconia is reported to be very effective to increase the oxygen mobility in ceria materials and increase the process of vacancy formation, thus contributing to stabilize the active phase and inhibit sintering [43,44].

TPR analysis are shown in Fig. 2. Origin software was used for the deconvolution of these TPR profiles. Green lines represent the experimental spectra. Several H_2 consumption steps are observed and correspond to the reduction of NiO particles of different size and/or different

Table 2
H_2 chemisorption results and calculated crystallite size of reduced Ni-La-Me catalysts.

Catalyst	Chemisorbed H_2 ($\mu L\ g_{cat}^{-1}$)	Ni dispersion (%)	Ni particle size (nm)	
			d_{CHEM}	d_{XRD}[a]
NiLaCe	163	0.73	112	20
NiLaCeZr	408	1.83	45	20
NiLaZr	442	1.98	41	18

[a] Calculated by the Scherrer equation from the (111) diffraction peak of Ni XRD pattern.

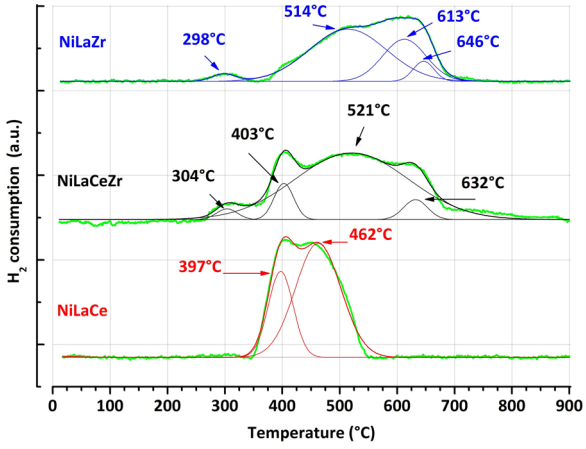

Fig. 2. TPR profile for Ni-La-Me catalysts.

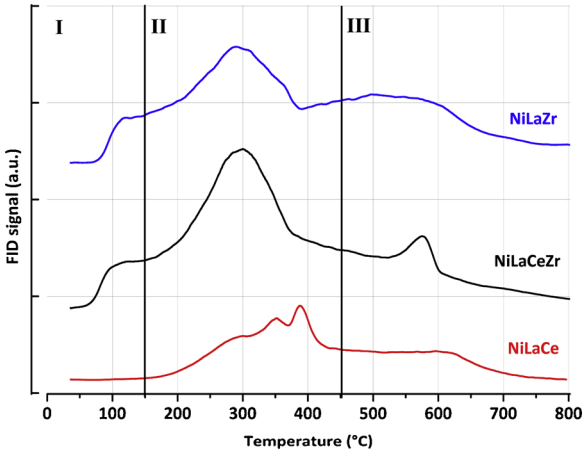

Fig. 3. TPD-CO_2 of reduced catalysts.

interaction degree with the mixed oxide. NiLaZr and NiLaCeZr catalysts show a first step from 270 °C to 350 °C which is attributed to the reduction of bulk NiO without interaction with the mixed oxide [42]. Deconvolution into Gaussian peaks allows to better characterize the contribution of the different Ni species.

Table 3 summarizes the relative contribution of deconvoluted signals. NiLaCe and NiLaCeZr show a deconvoluted peak centered on a temperature close to 400 °C that does not appear in NiLaZr and suggests that Ni reducibility is promoted by Ce as reported in the literature [45]. Peaks centered on temperatures higher than 500 °C appears only in NiLaZr (514 °C, 613 °C and 646 °C) and NiLaCeZr (521 °C and 632 °C) which suggests that they correspond to the reduction of Ni species having strong interactions with Zr. Differences between the influence of Ce and Zr on Ni reducibility can be related to their physical and chemical properties. CeO_2 is known to form nonstoichiometric oxides ($CeO_{(2-x)}$) at low oxygen partial pressures and temperatures above 773 K. Oxygen vacancies and high-ionic mobility exist in these compounds which gives them an enhanced redox ability [46].

Table 3 also shows that the reducibility of the 3 catalysts is higher than 100% corresponding to the whole amount of Ni. Theoretical uptake of H_2 for total reduction, assuming that NiO is stoichiometrically reduced to Ni, is 1.99 mmol g_{cat}^{-1}. NiLaCe and NiLaCeZr have the highest values (132% and 131% respectively) which can be ascribed to partial reduction of Ce^{+4} to Ce^{+3}. In the case of NiLaZr (116%), exceeding H_2 consumption could be ascribed to oxygen removal from mixed metal oxide accompanying the creation of oxygen defects mainly under the most severe reducing conditions at the range of highest temperatures [47].

Catalyst basicity was characterized by TPD-CO_2 since it has been reported that it limits the deposition of carbon and enhance the catalyst stability [48]. Fig. 3 shows that all 3 reduced catalysts present the most pronounced desorption peaks in the temperature range of medium basic strength between 150 °C and 450 °C. Additional signals are observed in the region of higher strength between 500 °C and 700 °C.

According to CO_2 uptakes shown in Table 4 NiLaCe has the smallest number of basic sites. NiLaCeZr has the greatest amount of basic adsorption sites both in medium and high strength regions. It has been reported that replacement of cerium ions by zirconium increases the oxygen mobility and the process of oxygen vacancies formation [28]. An increase in oxygen mobility can, in turn, increase the surface concentration of basic sites measured by CO_2 chemisorption [49]. A similar behavior derived from partial replacement of Ce by Zr could also take place in presence of La in the pyrochlore structures ($A_2B_2O_7$) here studied, leading to the increase of different basic sites [30]. NiLaCeZr has also the highest surface specific area, which in turn can also contribute to increase the amount of basic adsorption sites.

Table 4
CO_2 adsorption capacity of the reduced Ni-La-Me catalysts.

Catalyst	Basic sites (μgCO_2 /g catalyst)			
	Weak (I)	Medium (II)	Strong (III)	Total
NiLaCe	3.4	31.8	24.1	59.3
NiLaCeZr	14.0	58.5	45.5	117.9
NiLaZr	6.6	52.1	44.2	102.9

Table 5 summarizes the results obtained in CGSR and CGOSR tests at 650 °C. Glycerol conversion calculated from HPLC analysis of the liquid effluent, is almost complete for both kind of tests. Qualitative analyses of the liquid effluent in both reforming experiments revealed the presence of different intermediates such as acetaldehyde, methanol, ethanol, acetone, acetic acid, ethane-1,2-diol, propane-1,2-diol in agreement with those reported in the literature for glycerol steam reforming experiments [50].

Carbon conversion to gas products is about 74% in CGSR tests. This value is quite lower than those reported in a previous work of our group (90%), working with pure glycerol and other Ni-based catalysts under the same steam reforming conditions (atmospheric pressure, T = 650 °C, GHSV = 20 L h^{-1} g^{-1} and $WHSV_{CG}$ = 3 h^{-1}) [34]. The

Table 3
Total H_2 uptake and deconvoluted TPR profiles of calcined a Ni-La-Me catalysts.

Catalyst	Total H_2 uptake (mmol g_{cat}^{-1})	Reducibility (%)[a]	Deconvoluted peaks							
			1		2		3		4	
			T (°C)	H_2 uptake (%)	T (°C)	H_2 uptake (%)	T (°C)	H_2 uptake (%)	T (°C)	H_2 uptake (%)
NiLaCe	2.63	132	397	29.1	462	70.9	–	–	–	–
NiLaCeZr	2.61	131	304	2.5	403	7.9	521	84.3	632	5.3
NiLaZr	2.31	116	298	2.7	514	62.5	613	28.3	646	6.5

[a] Percentage reduction of Ni^{2+} ions measured by TPR.

Table 5
Gaseous products distribution in CGSR and CGOSR tests using Ni-La-Me catalysts (T = 650 °C, P = 1 bar, GHSV = 20 L h^{-1} g^{-1}, $WHSV_{CG}$ = 3 h^{-1}, TOS = 6 h).

Catalyst	Test	X_{Gly} (%)	$X_{C,GAS}$ (%)	$X_{C,LIQ}$ (%)	Product distribution (%) (dry basis)							
					H_2	CO	CO_2	CH_4	C_2H_4	C_2H_6	C_3H_6	C_3H_8
NiLaCe	CG	99.7	74.5	< 0.1	60.6	4.2	29.6	3.0	1.2	0.6	0.7	0.1
NiLaCeZr	SR	99.9	74.1	< 0.1	63.7	3.7	30.1	1.3	0.5	0.4	0.3	–
NiLaZr		99.7	73.6	< 0.1	62.8	3.9	30.0	1.7	0.7	0.4	0.4	0.1
NiLaCe	CG	99.8	90.4	< 0.1	59.7	3.1	36.4	0.7	0.1	–	–	–
NiLaCeZr	OSR	99.9	91.9	0.1	60.3	2.9	36.6	0.2	–	–	–	–
NiLaZr		99.9	90.9	0.1	59.9	2.8	36.9	0.4	–	–	–	–

lower value obtained with CGSR tests is attributed to a higher conversion to carbonaceous deposits. In this sense, pyrolysis reactions of CG impurities such as FAMEs lead to coke formation as reported by Dou et al. [11]

When O_2 was added to the feed in CGOSR experiments the conversion of carbon to gas products raised to approximately 91%. This higher value obtained in CGOSR experiments suggests that, in addition to the most reactive components (methanol and glycerol), FAMEs could also react under these reaction conditions leading to gas products typical of the reforming reactions [51]. As expected, the presence of O_2 in the feed promotes partial oxidation reactions leading to a decrease of H_2 and the increase of CO_2 concentration [52,53]. This higher CO_2 concentration could also promote the reverse WGSR consuming a fraction of hydrogen. It is also shown that CGOSR allows to obtain a gaseous mixture with much lower content of light hydrocarbons. This can be explained by an easier breaking of C—C bonds in the presence of O_2 and/or by the ocurrence of a more cleaned catalyst surface as a consequence of the lower amount of carbon deposits [54].

The performance of the catalysts was also tested in terms of H_2 yield as a function of time. As depicted in Fig. 4, Y_{H2} decreased continuously for all of them, thus revealing the existence of typical deactivation mechanisms such as carbon deposition and sintering [49,55]. Fouling due to physical deposition of the inorganic alkali compounds onto the catalyst surface can also result in blockage of sites and/or pores and at more advanced stages in particles disintegration. Nevertheless, alkali deposits may play a beneficial role since they favor steam gasification reactions due to their active catalytic role [46]. They can also exert a catalytic effect on the gasification of the carbonaceous deposits [47]. Fig. 4 also shows that catalysts are not affected in the same extent by deactivation. On one hand NiLaCe displays the greatest loss of activity with decays from 68% to 52% and from 84% to 70% in CGSR and CGOSR tests respectively. Deactivation by carbon formation could be specially favored on this catalyst because of its relative low basicity already shown in Fig. 3 and Table 4. The formation of C—C bonds on multiple Ni atoms sites is also expected to be favored on the NiLaCe catalyst containing the larger Ni crystallites [48,49]. In the same sense, interactions between both phases would be weakened in this catalyst, thus hindering carbon gasification reactions with water, carbon dioxide chemisorbed on the mixed oxide. NiLaCeZr showed the highest stability in both kind of tests which can be ascribed to a more efficient carbon removal from the boundaries of active sites due to its highest basicity and the smaller size of Ni crystallites. Other chemical and textural properties could also affect the catalyst stability. As it was already mentioned, the higher basicity of this catalyst would also involve a higher amount of oxygen vacancies with high mobility which would contribute to stabilize catalyst particles against sintering and coking [28,29,43,54,55]. Acidity is also reported to be involved in dehydration of oxygenated intermediates giving yield to olefins which are known to be coking precursors. It must also be pointed out that O_2 addition to the reagent feed improves H_2 yields although it would decay on a thermodynamic basis because of the higher CG conversion to gas products as well as that of the intermediates.

The quantity and nature of the carbon deposits formed in CGSR and

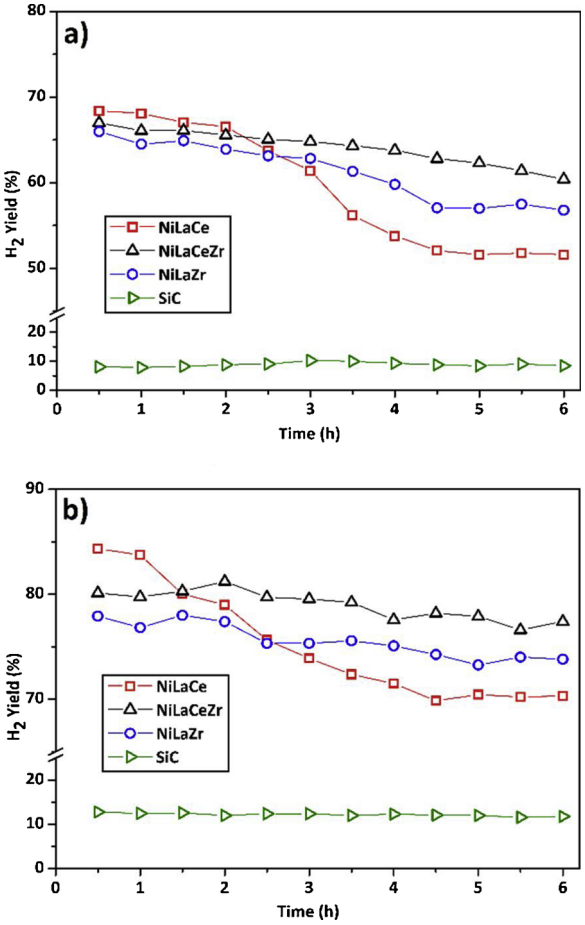

Fig. 4. Hydrogen yield of Ni-La-Me catalysts in: (a) CGSR and (b) CGOSR experiments.

CGOSR was investigated by TPO analysis of used catalysts and is shown in Fig. 5. The TPO profiles of the CGSR show three different oxidation zones: one at low temperature range (300–400 °C), the second in the range (400–550 °C) and the last one observed at high temperature range (550–720 °C). Several authors have reported the occurrence of different types of carbon deposits by reaction of oxygenates, with differences in its composition and/or its location on the catalyst [32,56–60]. The peaks at the lower combustion temperatures (< 450 °C) are ascribed to encapsulating carbon with amorphous nature close to the active metal particles and pointed out as the main responsible of catalyst deactivation by blocking metallic sites. The peaks at higher temperatures are usually associated to more structured carbon (filamentous and graphitic carbon) whose contribution to deactivation is hardly noticeable. Carbon deposition in SR reactions is a quite complex phenomenon since different mechanisms may be responsible for carbon formation. Ochoa et al. [60] provides a detailed discussion on the origin of the different types of carbon in the steam reforming of bio-oil oxygenates, such as

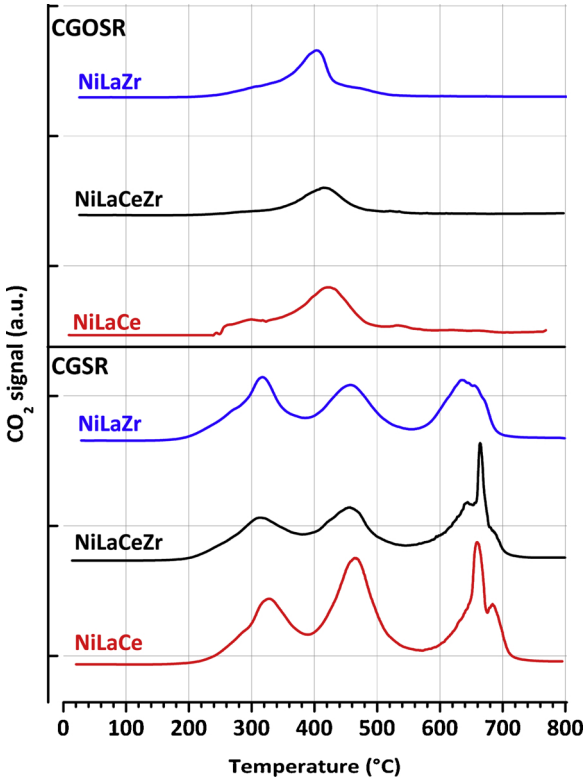

Fig. 5. TPO profiles of the used catalysts in CGSR and OCGSR.

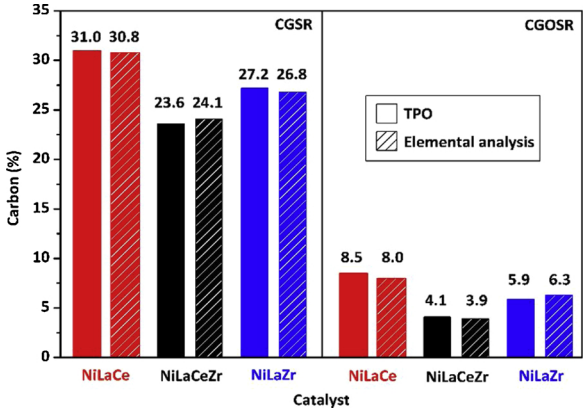

Fig. 6. Carbon contents of the used catalysts in CGSR and CGOSR.

alcohols, aldehydes, acids and phenols. They ascribe the formation of encapsulating carbon (which burns at low temperatures) to reactions of oxygenates in the reaction medium, which are adsorbed on the Ni sites and undergo further decomposition and/or condensation. Filamentous and graphitic carbon formation would occur from CO by the Boudouard reaction $2CO(g) \rightarrow C(s) + CO_2$ (g) and/or light hydrocarbons decomposition (CH_4, ethylene). Due to its more ordered structure and a less oxygenated composition with regard to the low temperature carbon, this type of carbon is harder to be burned. Other parameter, such as reaction temperature, steam to carbon ratio and Ni particle size also have a deep impact on the type and amount of carbon deposits. The TPO of the catalysts used in CGOSR show only one oxidation zone in the range (350–450 °C) demonstrating that all coke deposits have the same interaction with the catalyst indicating only one type of coke was produced. Oxygen is extremely reactive when compared to water and could easily react with glycerol and carbon precursors, mainly with those placed close to the metallic sites.

Carbon content in used catalysts determined by TPO and elemental

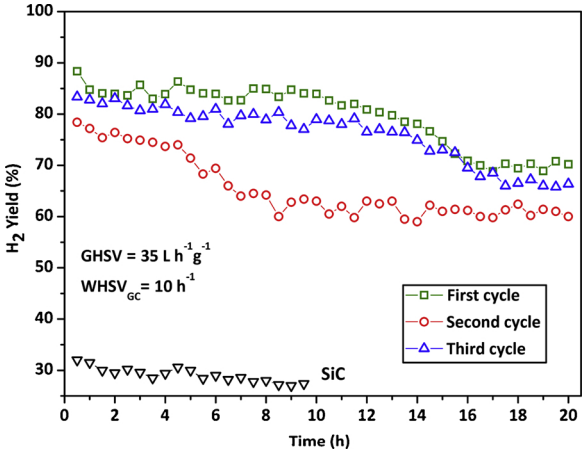

Fig. 7. H_2 yield during three cycles of deactivation/regeneration with NiLaCeZr catalyst. Reaction conditions: T = 650 °C, P = 1 bar, GHSV = 35 L h^{-1} g^{-1}, $WHSV_{CG}$ = 10 h^{-1}.

analysis are quite similar by both techniques and were summarized in Fig. 6. As shown, total amount of carbon content decreases in the following order: NiLaCe > NiLaZr > NiLaCeZr. This order is inversely related to that of catalyst basicity. It is well known that the stronger the catalyst basicity, the greater the amount of CO_2 adsorbed and thereby the greater the amount of carbon removed by the reaction of $C + CO_2 \leftrightarrow 2CO$ [61]. In the same way catalysts with the lower nickel particles size, observed in chemisorption experiments (NiLaZr and NiLaCeZr), exhibited lower carbon content since smaller nickel particles are reported to be more resistant to coking [62]. It is also shown that carbon deposition is significantly decreased by adding oxygen in the feed of CGOSR experiments.

The reuse of the NiLaCeZr catalyst in the CGOSR process was studied at lower contact times in order to detect more quickly the influence of changes in catalyst structure on its activity. Fig. 7 shows the decrease of H_2 yield from 89% to 70% in a first utilization of the fresh catalyst for 20 h. After catalyst regeneration with the O_2/Ar mixture (second cycle), the initial H_2 yield is partially recovered (79%) thus showing that carbon removal was not enough to fully regenerate the active sites. After the second regeneration involving the passage of the O_2/Ar mixture followed by passage of liquid water, the initial H_2 yield was about 85%, thus showing that the removal of alkali deposits contributes to a greater regeneration of the active sites.

The elemental composition of NiLaCeZr catalyst in different stages of the deactivation/regeneration study, obtained from the EDS data, are given in Table 6. For the fresh catalyst, the surface composition reasonably approximates the nominal value of each element. After the first O_2 regeneration carbon removal was almost complete. Potassium from the ashes contained in crude glycerol started to accumulate on catalyst surface. After 40 h of reaction, the second regeneration with O_2 was performed. Potassium concentration on catalyst surface was very noticeable reaching the value of 26.7 wt.%. Fermoso et al. [12] also observed alkali element (Na) present in carbon deposits, which comes from biodiesel transesterification catalyst, obtained after sorption enhanced steam reforming experiments. After washing the catalyst with water, surface composition of the catalyst returns to the initial values

A picture of the spent catalyst shows the presence of alkali deposits (Fig. 8a). XRD analysis show no significant changes in phase composition after the three 20-hours cycles of the deactivation/regeneration test (Fig. 8b). Before XRD analysis the spent catalyst was regenerated with O_2/Ar and washed with distilled water. Potassium carbonate was found after the second 20-hours cycle before washing the catalyst with water (Fig. 8c). $K_2CO_3.1.5H_2O$ presence might be explained by adsorption of moisture during XRD analysis. All these results reveal the high thermal and chemical stability of these mixed metal oxide

Table 6
Element weight and atomic percentage in NiLaCeZr catalyst. (average of three spectra).

Element	Fresh		After first O_2 regeneration		After second O_2 regeneration		After second O_2 regeneration + washed with distilled water	
	Wt %	At. %	Wt %	At. %	Wt %	At. %	Wt %	At. %
Ni	12.7	10.4	11.3	7.6	4.5	1.8	12.2	9.5
La	35.4	12.3	29.4	8.4	8.3	1.4	33.7	11.1
Ce	18,5	6.4	16.0	4.5	4.4	0.7	18.6	6.1
Zr	11.9	6.3	9.1	3.9	4.1	1.1	11.7	5.8
O	21.5	64.7	24.6	60.8	48.7	72.4	23.3	66.5
C	–	–	2.2	8.0	3.3	6.5	0.2	0.8
K	–	–	7.4	7.5	26.7	16.2	–	–

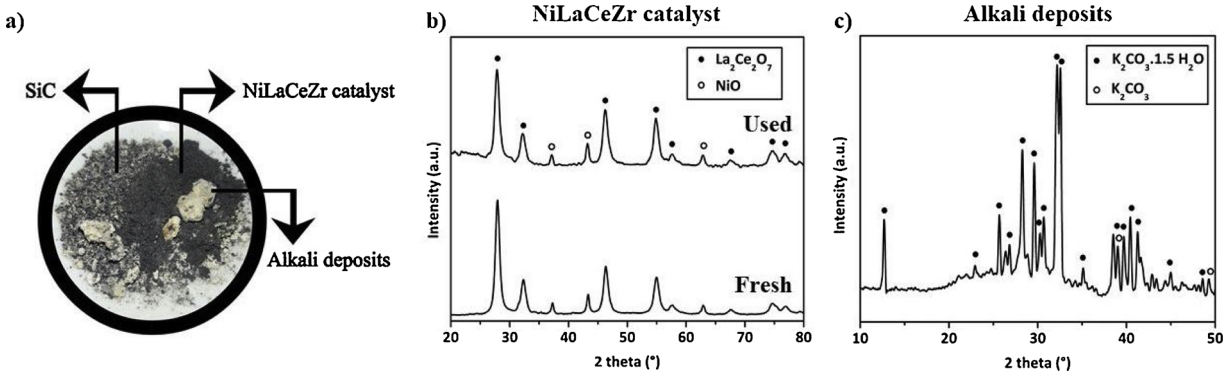

Fig. 8. Picture of the spent NiLaCeZr catalyst and XRD characterization.

materials, which makes them highly suitable for their use under the experimental conditions of the steam reforming process with presence of highly corrosive alkali compounds.

4. Conclusions

Ni-La-Me mixed oxides (Me: Ce and/or Zr) prepared by the Pechini-type polymerized complex route were tested as catalysts in the steam and oxidative steam reforming of crude glycerol at 650 °C. Catalysts obtained after a calcination temperature of 850 °C for 4 h lead contain two well defined phases, NiO and a $La_2Me_2O_7$ compound. NiO is easily reduced to metallic Ni on all catalysts in the presence of pure H_2 at 650 °C. Oxidative steam reforming allows to obtain the highest yields of gas products with all catalysts. The catalyst containing both Ce and Zr displayed the best catalytic performance in terms of H_2 yields and low deactivation which is ascribed to a more efficient carbon removal from the boundaries of active sites. Removal of carbon and alkali metals by simple procedures allows to a significant recovery of the catalytic activity without changes in the catalyst chemical and phase structure.

Acknowledgements

National Program for the Development of Basic Sciences (PEDECIBA-PNUD). Our thanks to ALUR (Alcoholes del Uruguay) for providing crude glycerol.

References

[1] Biofuels: Policies, Standards and Technologies, World Energy Council Regency House 1-4 Warwick Street London W1B 5LT United Kingdom, (2010).
[2] A.E. Atabani, A.S. Silitonga, I.A. Badruddin, T.M.I. Mahlia, H.H. Masjuki, S. Mekhilef, Renew. Sustain. Energy Rev. 16 (2012) 2070–2093.
[3] M.H. Hassan, M.A. Kalam, Procedia Eng. 56 (2013) 39–53.
[4] J. Silva, M.A. Soria, L. Madeira, Renew. Sustain. Energy Rev. 42 (2015) 1187–1213.
[5] Q. He, J. McNutt, J. Yang, Renew. Sustain. Energy Rev. 71 (2017) 63–76.
[6] N.D. Charisiou, K. Polychronopoulou, A. Asif, M.A. Goula, Surf. Coat. Technol. 352 (2018) 92–111.
[7] C.A. Schwengber, H.J. Alves, R.A. Schaffner, F.A. da Silva, R. Sequinel, V.R. Bach, et al., Renew. Sustain. Energy Rev. 58 (2016) 259–266.
[8] M. Greluk, P. Rybak, G. Słowik, M. Rotko, A. Machocki, Catal. Today 242 (2015) 50–59.
[9] H. Wang, X. Wang, M. Li, S. Li, S. Wang, X. Ma, Int. J. Hydrogen Energy 34 (2009) 5683–5690.
[10] M. Slinn, K. Kendall, C. Mallon, J. Andrews, Bioresour. Technol. 99 (2008) 5851–5858.
[11] B. Dou, G.L. Rickett, V. Dupont, P.T. Williams, H. Chen, Y. Ding, M. Ghadiri, Bioresour. Technol. 101 (2010) 2436–2442.
[12] J. Fermoso, L. He, D. Chen, Int. J. Hydrogen Energy 37 (2012) 14047–14054.
[13] J. Remón, V. Mercado, L. García, J. Arauzo, Fuel Process. Technol. 138 (2015) 325–336.
[14] J. Remón, C. Jarauta-Córdoba, L. García, J. Arauzo, Fuel Process. Technol. 145 (2016) 130–147.
[15] S. Veiga, J. Bussi, Energ. Convers. Manag. 141 (2017) 79–84.
[16] S. Veiga, R. Faccio, D. Segobia, C. Apesteguía, J. Bussi, Int. J. Hydrogen Energy 42 (2017) 30525–30534.
[17] E. Sánchez, M.A. D'Angelo, R.A. Comelli, Int. J. Hydrogen Energy 35 (2010) 5902–5907.
[18] S. Adhikari, S.D. Fernando, A. Haryanto, Catal. Today 129 (2007) 355–364.
[19] N.D. Charisiou, K.N. Papageridis, G. Siakavelas, L. Tzounis, K. Kousi, M.A. Baker, S.J. Hinder, V. Sebastian, K. Polychronopoulou, M.A. Goula, Top. Catal. 60 (2017) 1226–1250.
[20] A. Iriondo, V.L. Barrio, J.F. Cambra, P.L. Arias, M.B. Guémez, R.M. Navarro, M.C. Sánchez-Sánchez, J.L.G. Fierro, Top. Catal. 49 (2008) 46–58.
[21] M.H. Youn, J.G. Seo, K.M. Cho, J.C. Jung, H. Kim, K.W. La, Korean J. Chem. Eng. 25 (2008) 236–238.
[22] M.H. Youn, J.G. Seo, I.K. Song, Int. J. Hydrogen Energy 35 (2010) 3490–3498.
[23] B. Zhang, X. Tang, Y. Li, Y. Xu, W. Shen, Int. J. Hydrogen Energy 32 (2007) 2367–2373.
[24] H.S. Roh, I.H. Eum, D.W. Jeong, Renew. Energy 42 (2012) 212–216.
[25] E. Gallegos-Suárez, A. Guerrero-Ruiz, M. Fernández-García, I. Rodríguez-Ramos, A. Kubacka, Appl. Catal. B 165 (2015) 139–148.
[26] D. Srinivas, C.V.V. Satyanarayana, H.S. Potdar, P. Ratnasamy, Appl. Catal. A Gen. 246 (2003) 323–334.
[27] Ch.D. Dave, K.K. Pant, Renew. Energy 36 (11) (2011) 3195–3202.
[28] G. Nahar, V. Dupont, Renew. Sustain. Energy Rev. 32 (2014) 777–796.
[29] S. Shao, A.W. Shi, Ch.L. Liu, R.Z. Yang, W.S. Dong, Fuel Process. Technol. 125 (2014) 1–7.
[30] X. Li, L. Zhang, Ch. Zhang, M. Zhao, M. Gong, Y. Chen, J. Rare Earth 29 (6) (2011) 544–549.
[31] Y. Cui, V. Galvita, L. Rihko-Struckmann, H. Lorenz, K. Sundmacher, Appl. Catal. B 90 (2009) 29–37.
[32] C.A. Franchini, W. Aranzaez, A.M. Duarte de Farias, G. Pecchi, M.A. Fraga, Appl. Catal. B 147 (2014) 193–202.
[33] J. Bussi, M. Musso, S. Veiga, N. Bespalko, R. Faccio, A.C. Roger, Catal. Today 213 (2013) 42–49.
[34] S. Veiga, J. Bussi, Top. Catal. 59 (2) (2016) 186–195.
[35] M.M. Milanova, M. Kakihana, M. Arima, M. Yashima, M. Yoshimura, J. Alloys.

Compd. 242 (1996) 6–10.
[36] S. Gaur, D.J. Haynes, J.J. Spivey, Appl. Catal. A Gen. 403 (2011) 142–151.
[37] D.J. Haynes, D. Shekhawat, D.A. Berry, J. Zondlo, A. Roy, J.J. Spivey, Ceram. Int. 43 (2017) 16744–16752.
[38] C.W. Bale, E. Bélisle, Fact-Web Suite of Interactive Programs, www.factsage.com.
[39] W. Ma, X. Li, Y. Yin, H. Dong, Y. Bai, J. Liu, D. Nan, J. Wang, J. Alloys. Compd. 660 (2016) 85–92.
[40] M.R. Gogate, Appl. Catal. A Gen. 514 (2016) 203–213.
[41] Q. Liu, F. Gu, Z. Zhong, G. Xu, F. Su, RSC Adv. 6 (2016) 20979.
[42] N. Kumar, Z. Wang, S. Kanitkar, J.J. Spivey, Appl. Petrochem. Res. 6 (2016) 201–207.
[43] I.V. Yentekakis, G. Goula, P. Panagiotopoulou, S. Kampouri, M.J. Taylor, G. Kyriakou, R.M. Lambert, Appl. Catal. B 192 (2016) 357–364.
[44] V. Nichele, M. Signoretto, F. Menegazzo, A. Gallo, V. Dal Santo, G. Cruciani, G. Cerrato, Appl. Catal. B 111–112 (2012) 225–232.
[45] D. Ma, D. Mei, X. Li, M. Gong, Y. Chen, J. Rare Earths 24 (4) (2006) 451–455.
[46] B.M. Reddy, J.L.G. Fierro (Ed.), Redox Properties of Metal Oxides in Metal Oxides: Chemistry and Applications, Taylor & Francis, 2006Ch. 8.
[47] M.V. Ganduglia-Pirovano, A. Hofmann, J. Sauer, Surf. Sci. Rep. 62 (2007) 219–270.
[48] M. Fleys, Y. Simon, D. Swierczynski, A. Kiennemann, P. Marquaire, Energy Fuels 20 (2006) 2321–2329.
[49] J. Sehested, Catal. Today 111 (1) (2006) 103–110.
[50] L.F. Bobadilla, A. Penkova, F. Romero-Sarria, M.A. Centeno, J.A. Odriozola, Int. J. Hydrogen Energy 39 (2014) 5704–5712.
[51] M. Marquevich, F. Medina, D. Montané, Catal. Commun. 2 (2001) 119–124.
[52] S. de Lima, A. da Silva, L. da Costa, U. Graham, G. Jacobs, B. Davis, et al., J. Catal. 268 (2009) 268–281.
[53] V. Palma, C. Ruocco, E. Meloni, F. Gallucci, A. Ricca, Catal. Today 307 (2018) 175–188.
[54] M. Morales, M. Segarra, Appl. Catal. A Gen. 502 (2015) 305–331.
[55] M.D. Argyle, C.H. Bartholomew, Catalysts 5 (2015) 145–269.
[56] L.M. Martínez, M. Araque, J.C. Vargas, A.C. Roger, Appl. Catal. B 132–133 (2013) 499–510.
[57] L.F. Bobadilla, F. Romero-Sarria, M.A. Centeno, J.A. Odriozola, Int. J. Hydrogen Energy 46 (2016) 9234–9244.
[58] L.F. Bobadilla, A. Álvarez, M.I. Domínguez, F. Romero-Sarria, M.A. Centeno, M. Montes, J.A. Odriozola, Appl. Catal. B 123–124 (2012) 379–390.
[59] J. Vicente, J. Erena, C. Montero, M.J. Azkoiti, J. Bilbao, A.G. Gayubo, Int. J. Hydrogen Energy 39 (2014) 18820–18834.
[60] A. Ochoa, B. Aramburu, B. Valle, D.E. Resasco, J. Bilbao, A.G. Gayubo, P. Castaño, Green Chem. 19 (2017) 4315–4333.
[61] J.A. Calles, A. Carrero, A.J. Vizcaíno, L. García-Moreno, Catal. Today 227 (2014) 198–206.
[62] G. Wu, S. Li, C. Zhang, T. Wang, J. Gong, Appl. Catal. B 144 (2014) 277–285.